AGU PUBLICATIONS

Geophysical Research Letters

FRONTIER ARTICLE
10.1002/2015GL065271

Special Section:
First Results from the MAVEN Mission to Mars

Initial results from the MAVEN mission to Mars

Bruce M. Jakosky[1], Joseph M. Grebowsky[2], Janet G. Luhmann[3], and David A. Brain[1]

[1]Laboratory for Atmospheric and Space Physics, University of Colorado Boulder, Boulder, Colorado, USA, [2]NASA Goddard Space Flight Center, Greenbelt, Maryland, USA, [3]Space Sciences Laboratory, University of California, Berkeley, California, USA

Abstract The Mars Atmosphere and Volatile EvolutioN (MAVEN) Mars orbiter has been gathering information on the Mars upper atmosphere, ionosphere, and solar and solar wind interactions since its orbit insertion in September 2014. MAVEN's science goals are to understand processes driving the escape of atmospheric gases to space at the present epoch, and their variations with solar and local heliospheric conditions together with geographical and seasonal influences. This introduction and the accompanying articles provide a selection of key results obtained up to the time of writing, including measurements of the overall geometry and variability of the Martian magnetosphere, upper atmosphere, and ionosphere and their responses to interplanetary coronal mass ejections and solar energetic particle influxes. The ultimate goal is to use these results to determine the integrated loss to space through time and its role in overall Mars atmosphere evolution.

Key Points:
- MAVEN science results at Mars affect our understanding of the history of Mars volatiles
- Results integrate all aspects of the Mars upper atmosphere system

Correspondence to:
B. M. Jakosky,
bruce.jakosky@lasp.colorado.edu

Citation:
Jakosky, B. M., J. M. Grebowsky, J. G. Luhmann, and D. A. Brain (2015), Initial results from the MAVEN mission to Mars, *Geophys. Res. Lett.*, *42*, doi:10.1002/2015GL065271.

Received 7 JUL 2015
Accepted 19 AUG 2015

1. Introduction

The Mars Atmosphere and Volatile EvolutioN (MAVEN) mission is the first spacecraft devoted to studying the Mars upper atmosphere and ionosphere, its interactions with the Sun and the solar wind, and the consequent escape of atmospheric gases to space. By examining these processes, we can determine the physics underlying how gas is being lost to space today and then extrapolate back in time to determine the history of loss and the total amount of gas removed. This will let us determine whether loss to space was an important or possibly even the dominant process in driving the climate change that we infer has occurred based on the geological record [e.g., *Jakosky and Phillips*, 2001; *Carr*, 1996; *Bibring*, 2006]. While MAVEN is not the first spacecraft to examine some of these processes [e.g., *Hanson et al.*, 1977; *Mitchell et al.*, 2001; *Barabash et al.*, 2007], it has the most comprehensive payload suite designed to address these issues.

MAVEN launched from Cape Canaveral on 18 November 2013 and went into orbit at Mars on 21 September 2014. After a commissioning phase that included observations of the close passage of Comet Siding Spring, it began its 1 Earth year primary science mission on 16 November 2014. The MAVEN spacecraft is in an elliptical orbit with period of 4.5 h, periapsis altitude of ~150 km (with several campaigns down to ~125 km), and apoapsis ~6200 km. The inclination of 74° was chosen to allow precession of periapsis in both latitude and local solar time, providing substantial three-dimensional coverage of near-Mars space over the primary mission. Different types of observations are made during each portion of the orbit, taking advantage of both the in situ and remote sensing capabilities of MAVEN [*Jakosky et al.*, 2015a].

At this writing, MAVEN is about two thirds of the way through its primary mission. The behavior of the instruments is sufficiently well understood, and enough data have been collected, to allow us to obtain preliminary science results. These are reported in this collection of papers in *Geophysical Research Letters* and in a companion series of papers in *Science*.

In this paper, we summarize the key results and integrate them together into a broader understanding of the interplay between processes at Mars. The approach we have taken is to examine (i) the energetic drivers from the Sun that control processes in the Mars upper atmosphere, ionosphere, and magnetosphere; (ii) the composition, structure, and behavior of these regions and how they respond to the energetic drivers; and (iii) the measurements indicating loss to space. While it is premature to reach conclusions about the importance of loss processes over geologic time, we have made substantial progress in defining how these processes operate today.

2. Energetic Drivers

The inputs from the Sun consist of solar extreme ultraviolet radiation (EUV), the solar wind, and solar energetic particles that result from solar storms, coronal mass ejections (CMEs), and corotating interactive regions

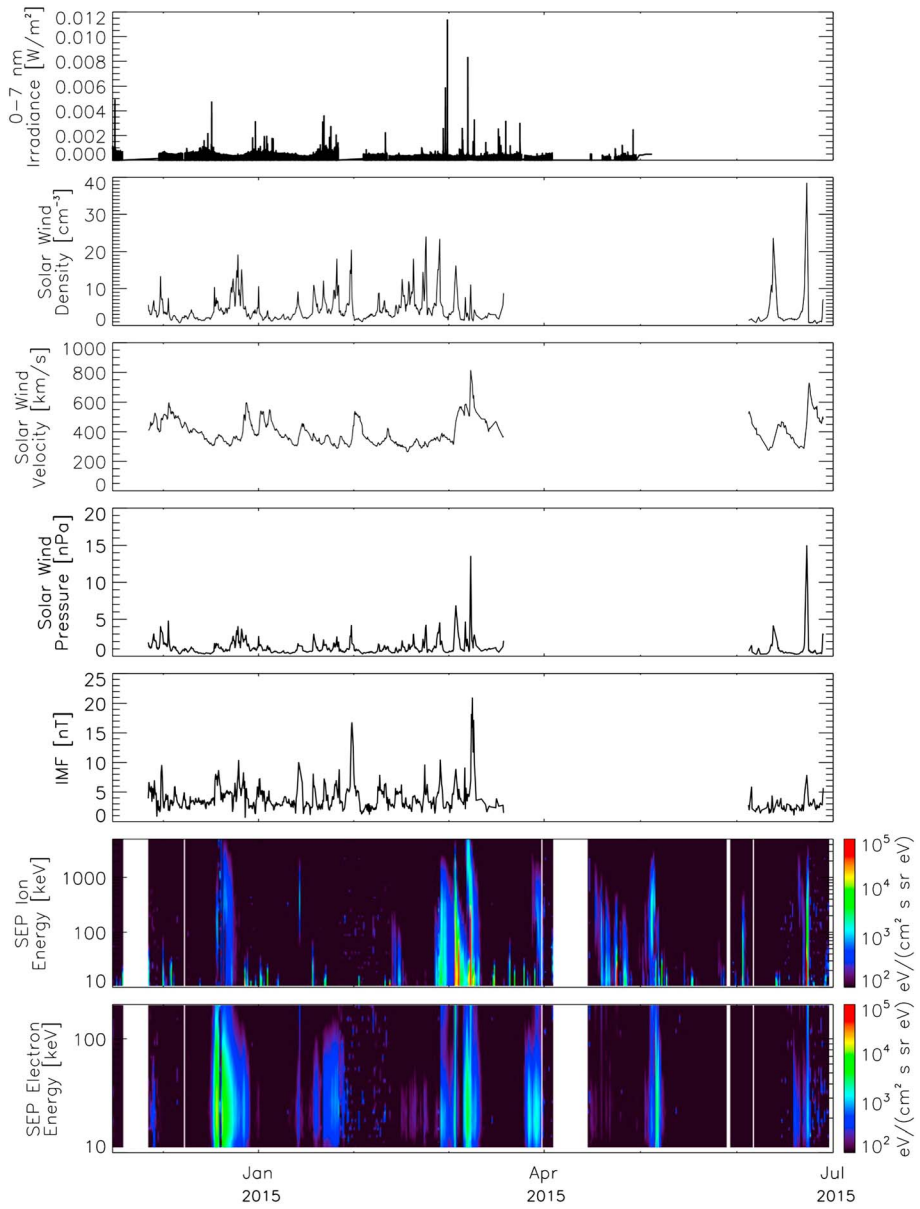

Figure 1. Solar energetic drivers of the Mars system, from start of primary science mission on 16 November 2014 through 30 June 2015. Panels show, from the top, solar EUV irradiance [*Eparvier et al.*, 2015]; solar wind density, velocity, and pressure [*Halekas et al.*, 2013]; interplanetary magnetic field [*Connerney et al.*, 2015]; and solar energetic ions and electrons [*Larson et al.*, 2015].

[see *Jakosky et al.*, 2015a, and references therein]. EUV light has a short-enough wavelength that it stimulates emission of electrons from atoms and molecules, creating the ionosphere. Reactions involving recombination of electrons and ions, or exchange of charge between different ions, drive both the chemistry and composition of the upper atmosphere and the photochemical escape of atoms to space.

The solar wind itself can "pick up" ions that are present at high altitudes, with the moving magnetic field of the solar wind creating an electric field that accelerates them. These pickup ions can be removed from the planet directly and can physically interact with both neutrals and ions in the upper atmosphere and drive escape through sputtering. The dramatic increase in solar wind speed, and the sudden impact of energetic electrons and protons from CMEs, can affect the upper atmosphere. They deposit energy at altitudes from the exobase (~200 km altitude) all the way down into the top regions of the lower atmosphere (as low as 50 km). The

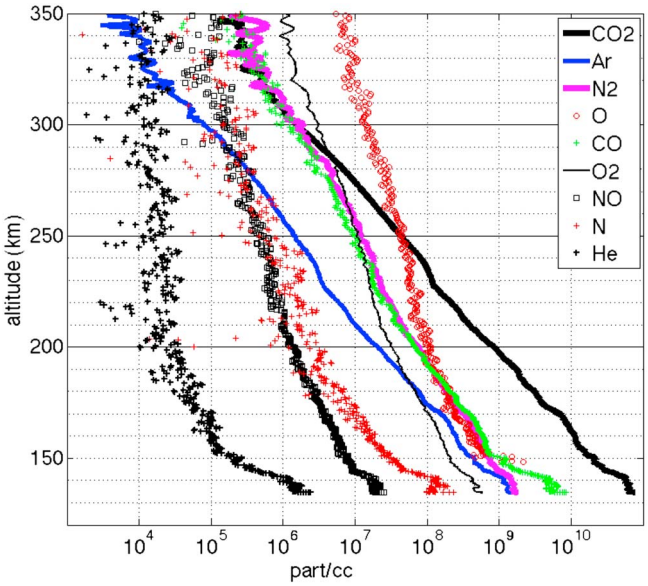

Figure 2. Example profiles of major measured in the Mars atmosphere [*Mahaffy et al.*, 2015].

resulting heating can cause the upper atmosphere to expand, change its interactions with the solar wind, and result in dramatic increases in escape rates.

By examining the effects of the changes in the energetic drivers, we can understand the individual processes responsible for controlling the upper atmosphere and the escape to space. All of the drivers vary throughout the 11 year solar cycle, and the solar cycle behaviors have changed throughout the history of the solar system. The escape rates can also vary depending on how the energetic drivers are affected by interactions with the magnetic fields associated with the locally magnetized regions of the crust.

Figure 1 shows solar energetic drivers as measured by MAVEN from the start of the primary mission up through the end of June 2015. Many of these drivers have been measured previously but never all together or with such high quality. The orbit precesses, with the periapsis location moving through both latitude and local solar time, so measurements of the upstream solar wind are not possible during periods of the mission when apoapsis is within the geomagnetic tail of Mars. There also are interruptions in observations twice each week when the spacecraft communicates with Earth, during a 3 week solar conjunction period when Mars is behind the Sun and not all instruments were operating normally, and for various spacecraft issues such as entry into safe mode.

Several solar events were observed at Mars, including a solar electron event just before Christmas 2014, three CME impacts at Mars in rapid succession in early March 2015, and several subsequent smaller events. Solar wind density varied by as much as an order of magnitude and solar wind velocity by a factor of 2. The corresponding solar wind dynamic pressure varied by more than an order of magnitude. The interplanetary magnetic field (IMF) also varied by a factor of 10, largely coincident with these other variations.

The impacts that these inputs and their variability have on Mars will be discussed below.

3. Upper Atmosphere and Ionosphere

The upper atmosphere nominally begins at the homopause altitude of ~120 km. Below this altitude, the atmosphere is well mixed, although some species such as H_2O can have variable mixing ratio because of condensation processes. Above the homopause, diffusion is more rapid than large-scale mixing, and each gas will have its own scale height. Figure 2 shows representative measurements from one orbit of the composition of the upper atmosphere [*Mahaffy et al.*, 2015]. MAVEN makes in situ measurements along a long orbital path near periapsis; although the measurements are shown as a function of altitude, they convolve altitude and horizontal trends. CO_2 is the dominant species at the lowest altitudes, commensurate with its comprising 95% of the lower atmosphere. However, at higher altitudes, O, O_2, N, and N_2 rapidly increase in relative abundance due to their lower masses (16, 32, 14, and 28 amu, respectively, relative to CO_2's 44) and resulting larger-scale heights [e.g., *Nier and McElroy*, 1977]. Argon, at mass 40, increases less rapidly. Above 300 km, atomic O is the dominant gas, followed by O_2 and N_2. Gases such as O, N, CO, O_2, and NO represent photodissociation products from the breakup of H_2O, CO_2, and N_2; as such, they are tracers of photochemical processes in both the lower and upper atmospheres [see *Yung et al.*, 1988].

MAVEN was designed to make measurements down to the vicinity of the homopause. Extrapolating N_2 and Ar mixing ratios downward until they match the measurements made in the lower atmosphere by the *Curiosity*

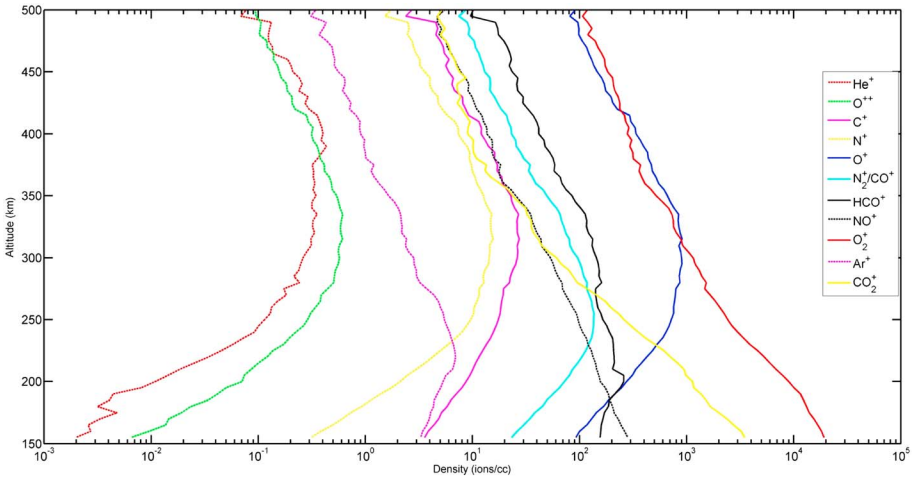

Figure 3. Example profile of major ions measured in the Mars ionosphere [*Benna et al.*, 2015b].

rover allows determination of the homopause altitude. Doing this yields a nominal altitude of 125 km, very similar to the 120 km altitude inferred using the same approach from the *Viking* 1 and 2 lander entry measurements [*Mahaffy et al.*, 2015]. Through the mission, MAVEN will be able to determine this altitude at multiple locations and local times; its variations will be important for understanding, for example, upward propagating waves that drive mixing and that also deposit energy into the upper atmosphere [e.g., *Leovy*, 1982].

The exobase altitude affects escape to space. It is the altitude above which an upward moving atom or molecule would be unlikely to hit something else before leaving the planet; the vicinity of the exobase represents a key source region for escaping atoms. For a typical constituent collision cross section of 3×10^{-15} cm^2, the exobase occurs where the integrated column abundance is the inverse of this, $\sim 3 \times 10^{14}$ cm^{-2}. The scale height of the atmosphere can be determined from the slope of the CO_2 abundance in Figure 2, about 18 km. This yields an exobase at an altitude at which the number density is $\sim 2 \times 10^8$ cm^{-3}, or about 200 km. This altitude also is expected to vary with location and season.

Figure 3 shows the major ions measured by MAVEN [*Benna et al.*, 2015b]. Although smaller in number, the ions are important for three reasons: (i) The recombination of electrons and molecular ions can release sufficient energy to break the molecule apart, leaving the atomic fragments with enough energy to escape from Mars. This dissociative recombination may have been important especially in the loss of O and N from the planet through time. (ii) The presence of an ionosphere affects how the solar wind interacts with Mars, due to the flow of ions and the magnetic field embedded in the solar wind. This flow can induce currents in the ionosphere, changing the interactions and controlling how the solar wind strips gas to space. And, (iii) much of the loss of atmospheric gas to space involves these ions, either stripped directly to space or causing loss by reimpact with the upper atmosphere near the exobase.

The abundances of O_2^+ and N_2^+ control their loss by dissociative recombination, and they are two of the most abundant ions (although N_2^+ cannot yet be distinguished from CO^+ due to their similar masses). In addition, MAVEN has discovered a wide range of hydrogen-bearing ions in the upper atmosphere [*Benna et al.*, 2015b]. These are indicative of a complex suite of chemical processes, plausibly driven by photodissociation of water in the upper atmosphere. Thus, it appears that water is transported readily into the upper atmosphere, despite the occurrence of cold traps in the middle atmosphere that should cause it to condense into ice grains that would settle out gravitationally.

The ionosphere is formed on the dayside by EUV photoionization of atmospheric molecules. Dissociative recombination of ions with the electrons occurs rapidly, such that the ionosphere largely disappears on the nightside. Figure 4 shows the variation of several key species as a function of solar zenith angle (SZA).

The transition to the nightside-depleted state of the ionosphere is shown in Figure 5. Electron densities and temperatures are shown on the nightside, at SZA from 110° to nearly 180° [*Fowler et al.*, 2015]. (At the altitude

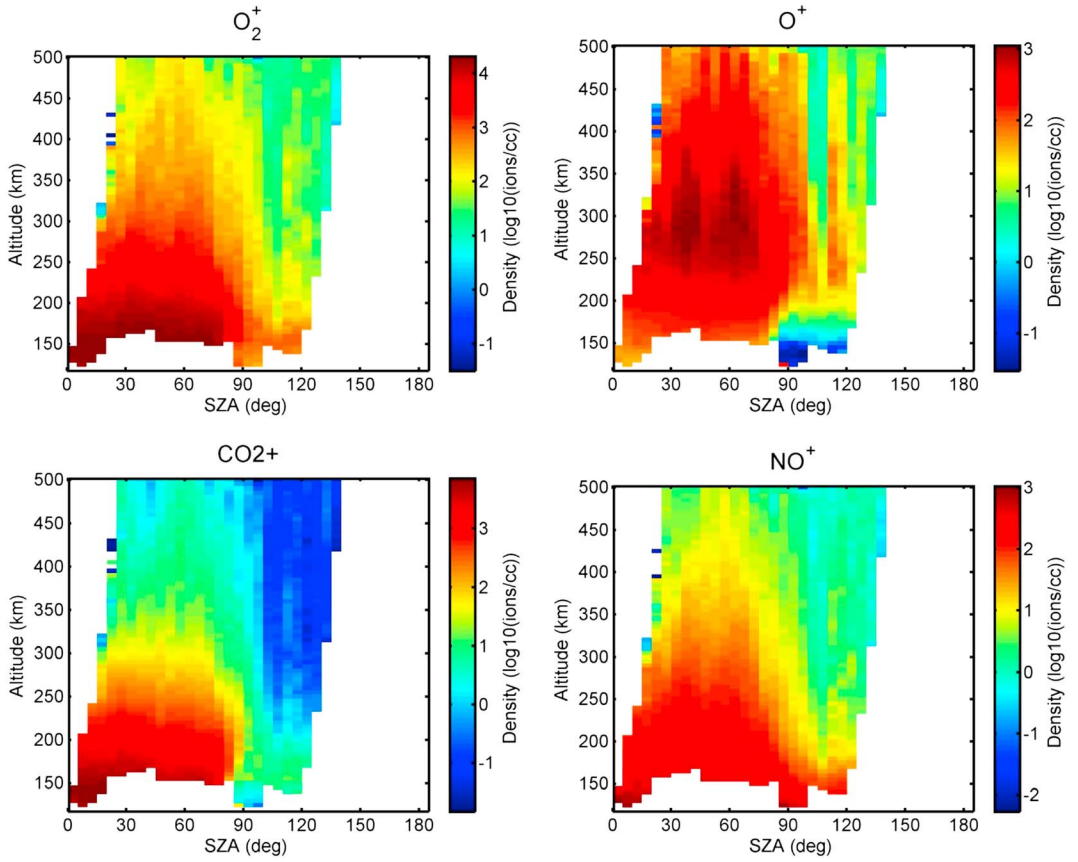

Figure 4. Distribution of key ions measured by the Neutral Gas and Ion Mass Spectrometer as a function of solar zenith angle (SZA). From *Benna et al.* [2015b].

of the ionosphere, gas is not shadowed from the Sun by the planet until a SZA of ~110°, unlike at the surface where anything beyond 90° is in shadow.) Electron temperature is important as it controls the dissociative recombination rate (and thereby the ion loss and the disappearance of the ionosphere) [see *Fox and Hać*, 2009] but also, along with the ion temperature, the plasma scale height. Electron density and temperature vary across the nightside due to recombination that removes ions and electrons, impact of solar particles and electrons that ionizes particles, and transport from the dayside to the nightside. Diurnal trends shown here through the night are complicated by the viewing geometry, which convolves local time, latitude, and SZA in complex ways.

In addition to the ions that are indicative of chemical processes related to the major components of the atmosphere, MAVEN has observed metal ions forming a discrete ionospheric layer. These were first seen following the close approach of Comet Siding Spring [*Schneider et al.*, 2015a; *Benna et al.*, 2015a] and were produced by the burn-up and ionization of dust debris from the comet; these ions disappeared in a matter of only days. During MAVEN's first deep-dip campaign to lower altitudes, metal ions were again detected. As there was no comet passage near that time, these ions must be the longer-lived background ionospheric layer produced continually by incoming interplanetary dust. This layer was hypothesized to exist at Mars, as it does at Earth, based on *Mars Express* radio-occultation measurements of the electron density [*Pätzold et al.*, 2005]; the ion metal species associated with such ionization had not previously been observed.

Mars also has an extended corona of energetic atomic species surrounding it [see *Anderson and Hord*, 1971; *Paxton and Anderson*, 1992]. MAVEN has observed the coronae produced from H, C, and O atoms, representing breakup products of the key climate-related gases CO_2 and H_2O. These coronae are formed by dissociative recombination and sputtering processes that give atoms more energy than they would have from thermal energy alone, but insufficient energy to escape the planet. They are

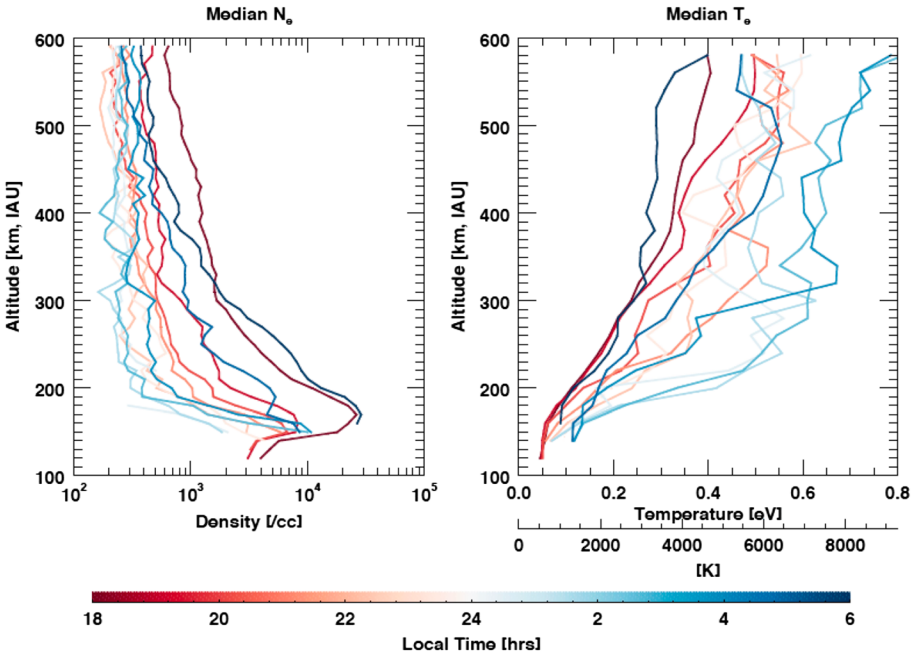

Figure 5. Electron temperature and number density measured by MAVEN on the Mars nightside ionosphere and shown binned in solar zenith angle. From *Fowler et al.* [2015].

bound in extended, noncollisional orbits and represent an additional source region for escaping gas. Figure 6 shows MAVEN images of these coronae [*Deighan et al.*, 2015; *Chaffin et al.*, 2015]. The H corona extends to at least 10 Mars radii (10 R_M), while the heavier O and C coronae are more tightly bound. The H distribution cannot be explained by a simple radially symmetric bound gas described by a single temperature, as depicted in the figure; there must be multiple components having different temperatures and thereby reflecting multiple processes operating on the atoms [*Chaffin et al.*, 2015].

4. Magnetosphere

The "magnetosphere" of Mars is formed when the solar wind encounters the obstacle presented by the combined upper atmosphere, ionosphere, and planetary crustal magnetic fields. The solar wind is traveling at supersonic velocities; as it first encounters the planet, it forms a shock wave (the bow shock) in which the solar wind is heated and transitions to subsonic flow. In this transition region between the bow shock and the obstacle, termed the "magnetosheath," some of the solar wind is deflected, but some of it interacts directly with the planet's atmosphere and ionosphere.

MAVEN has obtained coverage of the bow shock and magnetosheath that has allowed their properties to be characterized, including magnetic field measurements that had not been made previously. Figure 7 shows the average magnetic field and solar wind ion density in this region of the Mars-solar wind interaction for the period covered by the mission to date [*Halekas et al.*, 2015; *Connerney et al.*, 2015]. The shock-related density compression is clearly seen as is the density pileup at the nose of the Mars obstacle boundary, known from previous observational analyses as the magnetic pileup boundary.

Figure 7 (bottom two) shows the influence of the solar wind dynamic pressure on the bow shock location and magnetosheath densities. During periods of high pressure, the solar wind forces the obstacle boundary to lower altitudes than is typical. The solar wind pressure can move the location of the bow shock by as much as half the radius of Mars. In addition, the rotation of Mars exposes regions having different strengths of crustal magnetization [*Acuna et al.*, 2001], which, combined with the interplanetary magnetic field orientation, changes the effective size and shape of the Mars obstacle. The resulting effects of planetary rotation and

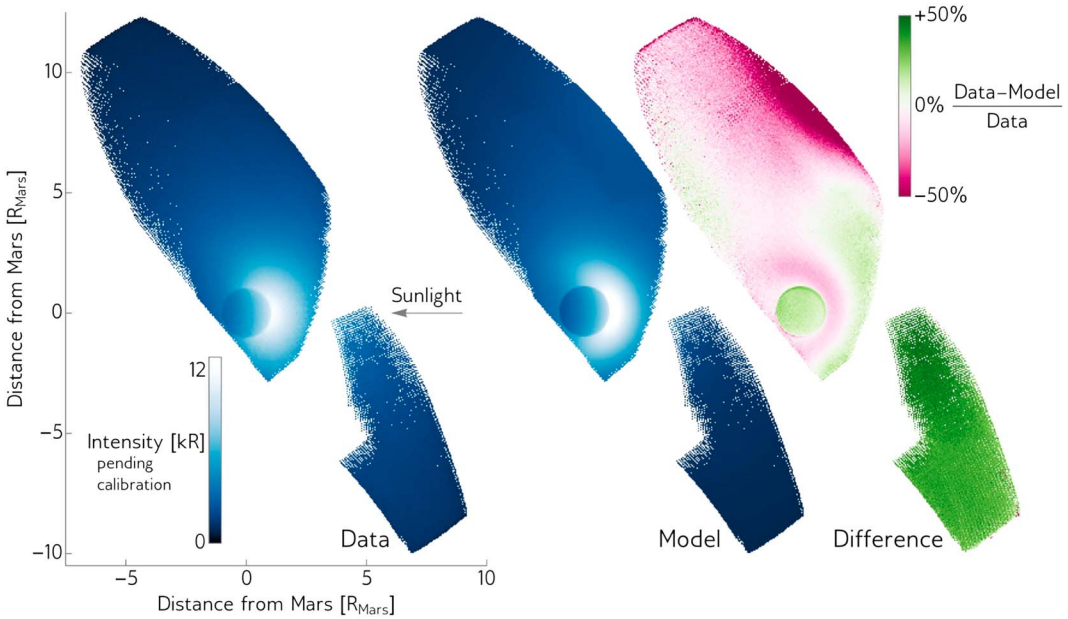

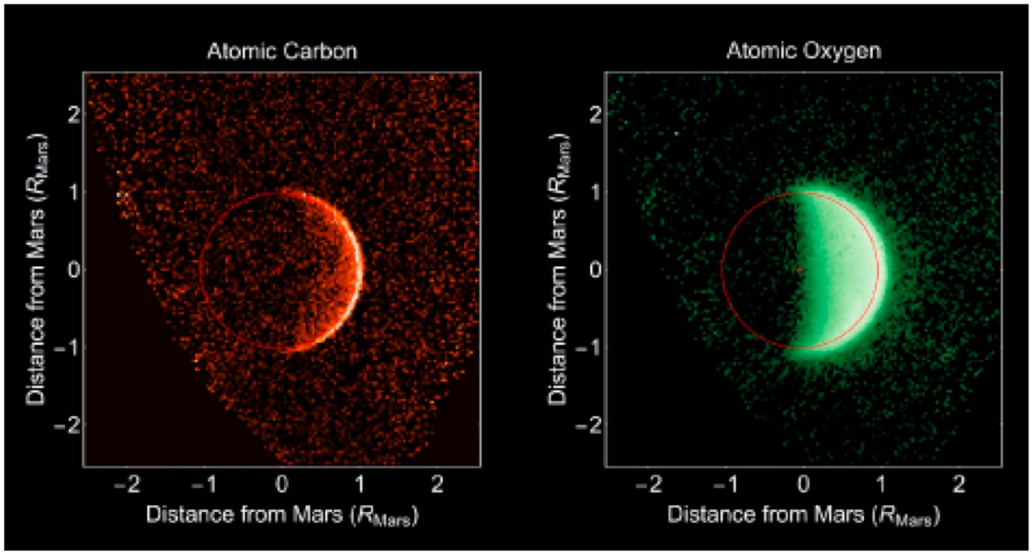

Figure 6. Coronae comprised of atomic (bottom) C and O and (top) H. Shown with H coronae are the results of the best fitting single-component model and the difference between the model and observations; systematic deviations between the model and observations require there to be multiple components in the corona. From *Deighan et al.* [2015] and *Chaffin et al.* [2015].

the changing solar wind conditions make this boundary a very diverse and dynamic entity [*Brain et al.*, 2005; *Lundin et al.*, 2011]. However, in spite of this complicated picture of Mars, the details of the MAVEN plasma and field measurements can be reproduced surprisingly well with a global magnetohydrodynamic (MHD) model of the solar wind interaction [*Ma et al.*, 2015].

Not all of the solar wind is stopped at the Mars obstacle boundary. Some penetrates the ionosphere-magnetosphere boundary (IMB) and reaches altitudes deep within the upper atmosphere [*Halekas et al.*, 2015]. The mechanism of penetration is thought to involve charge exchange reactions. A fraction of solar wind protons will exchange charge with hydrogen atoms in the extended corona outside of the bow shock; these retain their original velocity as fast-moving neutral atoms and can penetrate unimpeded through the IMB. They can then charge exchange again in the upper atmosphere, where they are again observed as ions

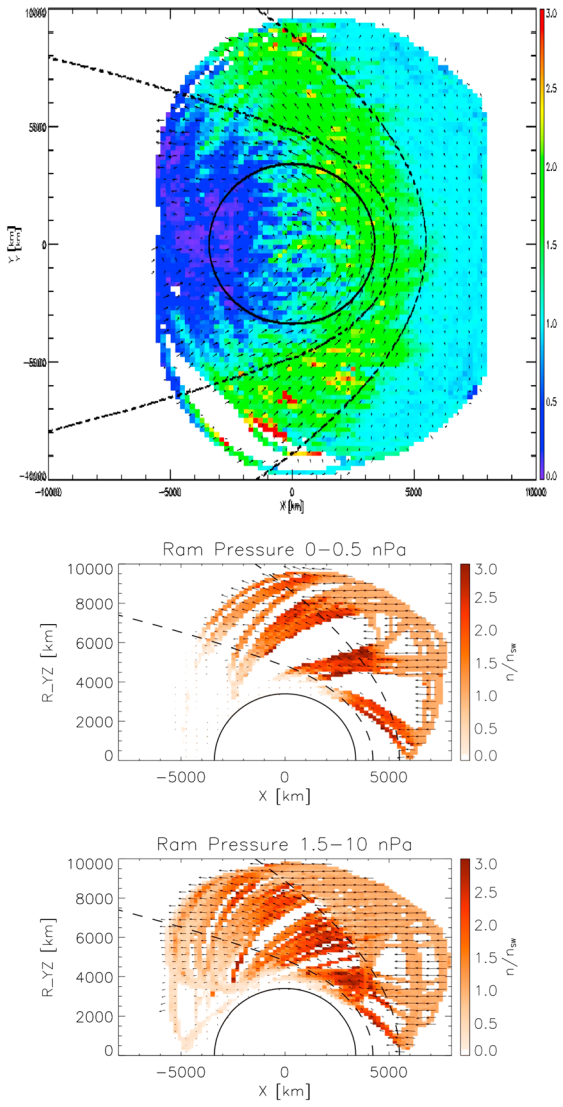

Figure 7. Measured solar wind properties showing the location of the bow shock, magnetosheath, and ionosphere-magnetosphere boundary. (top) Average of all measurements to date. (bottom two) The results sorted into the highest and lowest solar wind pressures.

that still have their original velocity. Collisions of these energetic atoms with the components of the upper atmosphere represent a means of heating the latter more deeply than a solar wind proton itself could directly accomplish [*Halekas et al.*, 2015].

Energetic ions and electrons from the solar wind can also energize upper atmospheric molecules and atoms by collision. This stimulation by ion/electron impact mimics that which occurs from absorption of solar EUV radiation. These excited molecules lose that energy by giving off light at wavelengths characteristic of the excited species. When stimulation was by solar EUV, the emitted light is referred to as dayglow. When stimulated by externally accelerated electrons/ions, the light is known as the aurora. Aurora have been observed previously at Mars from the Mars Express spacecraft, in isolated regions between highly magnetized crustal regions where incoming solar particles are focused by the local magnetic fields [*Bertaux et al.*, 2005]. MAVEN has discovered auroral emission distributed broadly over large areas and not associated with crustal magnetic fields [*Schneider et al.*, 2015b]. This latter emission is referred to as the "diffuse aurora" to distinguish it from the "discrete aurora" observed by Mars Express. The diffuse aurora occurs where particles enter the Mars upper atmosphere from outside, presumably following magnetic field lines that connect directly from the solar wind to the planet. The impact of the particles producing this diffuse aurora also provides energy that heats the upper atmosphere.

The magnetic field from the solar wind can affect planetary ions already present in the solar wind, magnetosheath, and ionosphere. A planetary ion sees the solar wind magnetic field moving with respect to the ion at the velocity of the solar wind. The moving magnetic field creates an electric field given by $\mathbf{E} = -\mathbf{v} \times \mathbf{B}$. This electric field will accelerate these ions and can even take them up to the escape velocity (~5 km/s for Mars) and larger, resulting in their loss to space. The solar wind velocity and magnetic field vector are typically close to the plane of Mars' orbit around the Sun, and the electric field is perpendicular to these, or roughly perpendicular to the orbital plane. As a result, the ions that are "picked up" at high altitudes initially move away from Mars along roughly northward or southward trajectories. However, the magnetic field makes them gyrate around it, and so the actual trajectories resemble large arcs in the space sampled by MAVEN. Because of this spatial distribution, these accelerated ions are referred to here and elsewhere as a "polar plume" of escaping ions [*Fang et al.*, 2008; *Dubinin et al.*, 2011].

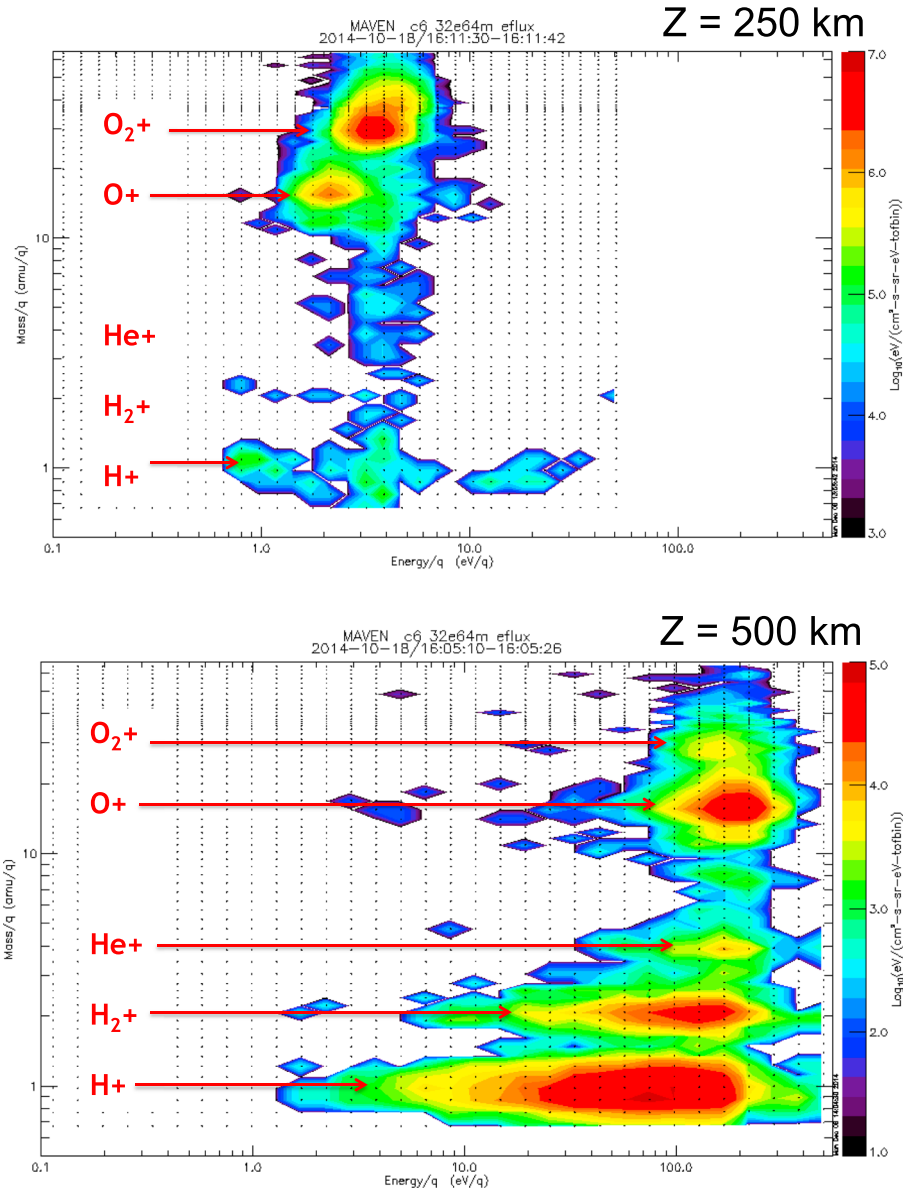

Figure 8. (top and bottom) Suprathermal and Thermal Ion Composition (STATIC) measurements at two altitudes where the polar plume is expected to be observed, showing acceleration to higher energies due to the solar wind-induced electric field. From *McFadden et al.* [2015].

Figure 8 shows the acceleration of ions with increasing altitude measured in the vicinity of the polar plume [*McFadden et al.*, 2015]. At low altitudes (Figure 8, top), all of the ions have essentially thermal energies, consistent with there having been no acceleration yet by the electric field. Figure 8 (bottom) contains measurements at higher altitudes and shows that the ions have now been accelerated to energies greater than that required to escape. The increased spread in energy for the lighter species here suggests that the acceleration is still acting.

Figure 9 shows a collection of all equivalent measurements made when the spacecraft was in an orientation that would allow it to observe the polar plume ions [*Y. Dong et al.*, 2015]. The measurements are plotted in what is known as Mars-Sun-Electric Field (MSE) coordinates. This system is aligned with the direction of the $-\mathbf{v}\times\mathbf{B}$ electric field, since that governs the motion of ions: the x axis is pointed toward the Sun so that the solar wind velocity vector is along $-x$, y is the direction closest to the upstream magnetic field component perpendicular to x, and z is then along the electric field vector. In this coordinate system, the average

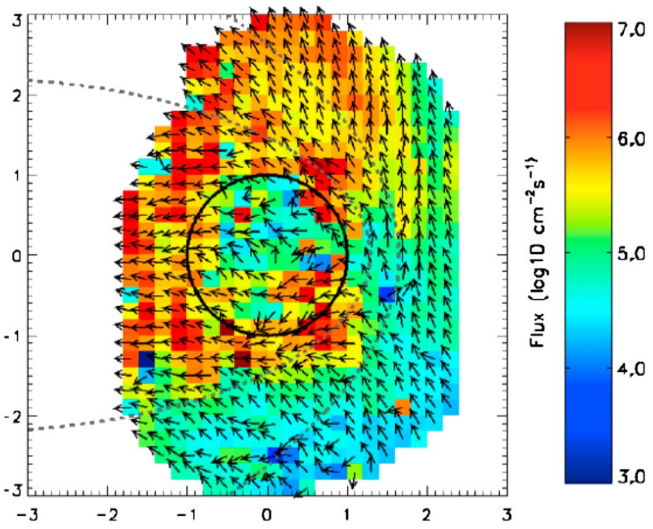

Figure 9. Average density and velocity vector of ions measured by STATIC, shown in MSE coordinates, and including only those observations when STATIC was oriented to be able to detect the polar plume flow. From *C. Dong et al.* [2015].

direction of motion of observed planetary oxygen ions, shown by the arrows, is clearly controlled by the electric field. Upward moving O^+ ions in the bottom half of the space can hit the planet, while those in the top half are accelerated upward and can escape. These data suggest that the polar plume makes a significant contribution to the total escape rate of planetary O^+ ions.

The behavior of the pickup ions in the other locations in Figure 9 is also important. In particular, those that impact the atmosphere mainly in the MSE southern hemisphere can sputter away atmospheric gas by transferring their energy, via collisions, to other particles in the vicinity of the exobase [*Luhmann and Kozyra*, 1991]. While we can infer from these observations that some of these solar wind-energized O^+ ions strike the atmosphere, we are still investigating the evidence for this sputtering effect. Only then will we be able to assess this process' potential importance over time [*Luhmann et al.*, 1992; *Johnson,* 1994].

MAVEN has detected some of these pickup ions that had been produced upstream from Mars. Figure 10 shows the observations of high-energy ions made at a time when the spacecraft was upstream of the bow shock [see *Halekas et al.*, 2013]. Ion mass cannot be readily determined from these observations, but the abundances and high energies of these ions indicate that they are likely to be O^+ pickup ions. The formation of such pickup ions can be modeled, based on a model that assumes photoionization of the extended neutral oxygen corona surrounding Mars and subsequent acceleration by the solar wind electric field. The resulting distribution of high-energy ions, convolved with the field of view of the Solar Wind Ion Analyzer (SWIA) instrument at the time of the observations, tells us which pickup ions can be detected by the instrument. The output of such a model is shown in Figure 10 along with the measurements [*Rahmati et al.*, 2015]. The very good correspondence gives us confidence that indeed, pickup oxygen ions from the Mars O corona are being observed and let us quantify their formation and subsequent behavior.

5. Loss to Space

Ideally, we would consider each loss process separately, determine the resulting escape rates, and sum them up to get a total loss rate. Sufficient measurements have not yet been made nor analyses carried out, to do that. However, we can begin to look at some of the escape mechanisms and rates.

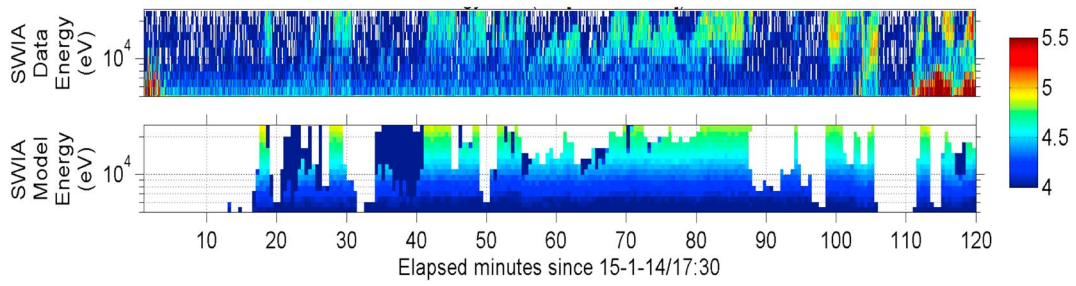

Figure 10. Energetic ions (top) measured by Solar Wind Ion Analyzer (SWIA) and (bottom) predicted by a model of pickup ion production and acceleration. From *Rahmati et al.* [2015].

MAVEN can measure directly the ions escaping from Mars. This is done numerically by taking an arbitrary surface enclosing Mars and counting the ions that are escaping each time the spacecraft passes through that surface [*Brain et al.*, 2015]. This can be done only over a long period so that the precession of the orbit allows sampling of different geographical locations, and the time variable IMF provides an even broader distribution in MSE coordinates. However, some of the ions that leave in one place may return immediately in another place, and some newly created ions upstream of Mars can impact onto Mars. In order to not double count these ions, one also has to count the incoming or returning ions and subtract this from the total. In doing this, it is easy to identify the regions of enhanced incoming ions, such as on the side of Mars facing into the solar wind; this region accretes many of the ions formed upstream of Mars, picked up, and impacting onto Mars. In addition, the polar plume and the general escape down the tail stand out as regions of enhanced loss. The polar plume accounts for roughly one third to one half of the total escaping ions for the period observed by MAVEN. This makes it potentially one of the important channels for escape from the planet, at least at the present [*C. Dong et al.*, 2015].

Loss will be increased during solar storm events, as the solar wind and energetic particle drivers are enhanced [see *Futaana et al.*, 2008; *Edberg et al.*, 2010]. MAVEN has observed Mars during one significant CME event, in early March 2015 [*Jakosky et al.*, 2015b]. It is difficult to measure the total escape enhancement, as observations over the several days of the event were extremely limited in geographical and MSE coverage. However, they indicate a significant increase, showing the largest instantaneous loss rates observed to date. Models of the interaction of the solar wind with the planet can be used to estimate the escape enhancement during CMEs, given that they provide a reasonably good match to the behavior during both quiet times and disturbed times. They suggest that roughly an order-of-magnitude increase in loss rates can occur during these events [*Jakosky et al.*, 2015b].

6. Upcoming Mission Activities

MAVEN observations and analyses do not yet give us a complete picture of solar interactions with Mars and the effects on loss to space. However, they do provide a significant advance beyond previous measurements in our ability to determine the current state of the upper atmosphere and ionosphere, the nature of the interactions with the Sun and the solar wind, and the ability of these processes to drive escape. During the rest of the MAVEN primary mission, we expect to be able to fill out the basic framework obtained so far, with additional observations and model analyses, and provide the details necessary to answer the science questions.

MAVEN has been approved for an initial 1 year extended mission. This extension will allow it to observe Mars for the second half of a Mars year, thereby completing the observations at all seasons and under different conditions of lower atmospheric dust loading and water vapor content and allowing it to continue measurements during the declining phase of the solar cycle. There has been an initial release of MAVEN data to the Mars science community via the Planetary Data System (PDS), and data are to be released subsequently at 3 month intervals.

This is an exciting time in understanding Martian aeronomy and the role played by loss to space in the changing Martian climate through time. The papers in these collections represent just the first glance at the results.

Acknowledgments

The MAVEN mission has been supported by NASA through its Mars Exploration Program. Planetary exploration is a "team sport," and the results presented here and in the accompanying papers represent the work of hundreds of scientists and engineers who designed, built, and operate the spacecraft and instruments and carried out the scientific analyses. We are indebted to them beyond words. We thank Christina Lee and Jasper Halekas for producing Figure 1.

The Editor thanks Larry Paxton and an anonymous reviewer for their assistance in evaluating this paper.

References

Acuna, M., et al. (2001), Magnetic field of Mars: Summary of results from the aerobraking and mapping orbits, *J. Geophys. Res.*, *106*, 23,403–23,417, doi:10.1029/2000JE001404.

Anderson, D. E., and C. W. Hord (1971), Mariner 6 and 7 Ultraviolet Spectrometer experiment: Analysis of hydrogen Lyman-alpha data, *J. Geophys. Res.*, *76*, 6666–6673, doi:10.1029/JA076i028p06666.

Barabash, S., A. Fedorov, R. Lundin, and J.-A. Sauvaud (2007), Martian atmospheric erosion rates, *Science*, *315*(5811), 501–503, doi:10.1126/science.1134358.

Benna, M., P. R. Mahaffy, J. M. Grebowsky, J. M. C. Plane, R. V. Yelle, and B. M. Jakosky (2015a), Metallic ions in the upper atmosphere of Mars from the passage of comet C/2013 A1 (Siding Spring), *Geophys. Res. Lett.*, *42*, 4670–4675, doi:10.1002/2015GL064159.

Benna, M., P. R. Mahaffy, J. M. Grebowsky, J. L. Fox, R. V. Yelle, and B. M. Jakosky (2015b), First measurements of composition and dynamics of the Martian ionosphere by MAVEN's Neutral Gas and Ion Mass Spectrometer, *Geophys. Res. Lett.*, *42*, doi:10.1002/2015GL066146.

Bertaux, J.-L., F. Leblanc, O. Witasse, E. Quemerais, J. Lilensten, S. A. Stern, B. Sandel, and O. Korablev (2005), Discovery of an aurora on Mars, *Nature*, *435*(7), 790–794, doi:10.1038/nature03603.

Bibring, J. P. (2006), Global mineralogical and aqueous Mars history derived from OMEGA/Mars Express data, *Science*, *312*(5772), 400–404, doi:10.1126/science.1122659.

Brain, D. A., J. S. Halekas, R. J. Lillis, D. L. Mitchell, R. P. Lin, and D. H. Crider (2005), Variability of the altitude of the Martian sheath, *Geophys. Res. Lett. 32*, L18203, doi:10.1029/2005GL023126.

Brain, D. A., et al. (2015), The spatial distribution of planetary ion fluxes near Mars observed by MAVEN, *Geophys. Res. Lett.*, *42*, doi:10.1002/2015GL065293.
Carr, M. H. (1996), *Water on Mars*, Oxford Univ. Press, New York.
Chaffin, M. S., et al. (2015), Three-dimensional structure in the Mars H corona revealed by IUVS on MAVEN, *Geophys. Res. Lett.*, *42*, doi:10.1002/2015GL065287.
Connerney, J., et al. (2015), First results of the MAVEN magnetic field investigation, *Geophys. Res. Lett.*, *42*, doi:10.1002/2015GL065366.
Deighan, J., et al. (2015), MAVEN IUVS observation of the hot oxygen corona at Mars, *Geophys. Res. Lett.*, *42*, doi:10.1002/2015GL065487.
Dong, C., et al. (2015), Multi-fluid MHD study of the solar wind interaction with Mars' upper atmosphere during the 2015 March 8th ICME event, *Geophys. Res. Lett.*, *42*, doi:10.1002/2015GL065944.
Dong, Y., X. Fang, D. A. Brain, J. P. McFadden, J. S. Halekas, J. E. Connerney, S. M. Curry, Y. Harada, J. G. Luhmann, and B. M. Jakosky (2015), Strong plume fluxes at Mars observed by MAVEN: An important planetary ion escape channel, *Geophys. Res. Lett.*, *42*, doi:10.1002/2015GL065346.
Dubinin, E., M. Fraenz, A. Fedorov, R. Lundin, N. Edberg, F. Duru, and O. Vaisberg (2011), Ion energization and escape on Mars and Venus, *Space Sci. Rev.*, *162*(1), 173–211, doi:10.1007/s11214-011-9831-7.
Edberg, N. J. T., H. Nilsson, A. O. Williams, M. Lester, S. E. Milan, S. W. H. Cowley, M. Fränz, S. Barabash, and Y. Futaana (2010), Pumping out the atmosphere of Mars through solar wind pressure pulses, *Geophys. Res. Lett.*, *37*, L03107, doi:10.1029/2009GL041814.
Eparvier, F. G., E. M. B. Thiemann, P. C. Chamberlin, and T. N. Woods (2015), Solar EUV irradiance at Mars: Why we're measuring it and why you should care, Lunar Planet. Sci. Conf., Abstract 3001, Houston, Tex.
Fang, X., M. W. Liemohn, A. F. Nagy, Y. Ma, D. L. De Zeeuw, J. U. Kozyra, and T. H. Zurbuchen (2008), Pickup oxygen ion velocity space and spatial distribution around Mars, *J. Geophys. Res.*, *113*, A02210, doi:10.1029/2007JA012736.
Fowler, C. M., et al. (2015), The first in-situ electron temperature and density measurements of the Martian nightside ionosphere, *Geophys. Res. Lett.*, *42*, doi:10.1002/2015GL065267.
Fox, J. L., and A. B. Hać (2009), Photochemical escape of oxygen from Mars: A comparison of the exobase approximation to a Monte Carlo method, *Icarus*, *204*(2), 527–544, doi:10.1016/j.icarus.2009.07.005.
Futaana, Y., et al. (2008), Mars Express and Venus Express multi-point observations of geoeffective solar flare events in December 2006, *Planet. Space Sci.*, *56*(6), 873–880, doi:10.1016/j.pss.2007.10.014.
Halekas, J. S., E. R. Taylor, G. Dalton, G. Johnson, D. W. Curtis, J. P. McFadden, D. L. Mitchell, R. P. Lin, and B. M. Jakosky (2013), The Solar Wind Ion Analyzer for MAVEN, *Space Sci. Rev.*, doi:10.1007/s11214-013-0029-z.
Halekas, J. S., et al. (2015), MAVEN observations of solar wind hydrogen deposition in the atmosphere of Mars, *Geophys. Res. Lett.*, *42*, doi:10.1002/2015GL064693.
Hanson, W. B., S. Sanatani, and D. R. Zuccaro (1977), The Martian ionosphere as observed by the Viking retarding potential analyzers, *J. Geophys. Res.*, *82*, 4351–4363, doi:10.1029/JS082i028p04351.
Jakosky, B. M., and R. J. Phillips (2001), Mars' volatile and climate history, *Nature*, *412*, 237–244.
Jakosky, B. M., et al. (2015a), The MAVEN mission to Mars, *Space Sci. Rev.*, doi:10.1007/s11214-015-0139-x.
Jakosky, B. M., et al. (2015b), MAVEN observations of the response of Mars to an interplanetary coronal mass ejection, *Science*, doi:10.1126/science.aad0210, in press.
Johnson, R. E. (1994), Plasma-induced sputtering of an atmosphere, *Space Sci. Rev.*, *69*(3), 215–253, doi:10.1007/BF02101697.
Larson, D. E., et al. (2015), The Solar Energetic Particle Experiment on MAVEN: First results, Lunar Planet. Sci. Conf., Abstract 2890, Houston, Tex.
Leovy, C. B. (1982), Control of the homopause level, *Icarus*, *50*, 311–321.
Luhmann, J., and J. U. Kozyra (1991), Dayside pickup oxygen ion precipitation at Venus and Mars—Spatial distributions, energy deposition and consequences, *J. Geophys. Res.*, *96*, 5457–5467, doi:10.1029/90JA01753.
Luhmann, J. G., R. E. Johnson, and M. H. G. Zhang (1992), Evolutionary impact of sputtering of the Martian atmosphere by O(+) pickup ions, *Geophys. Res. Lett.*, *19*, 2151–2154, doi:10.1029/92GL02485.
Lundin, R., S. Barabash, M. Yamauchi, H. Nilsson, D. Brain (2011), On the relation between plasma escape and the Martian crustal magnetic field, *Geophys. Res. Lett.*, *38*, L02102, doi:10.1029/2010GL046019.
Ma, Y. J., et al. (2015), MHD model results of solar wind interaction with Mars and comparison with MAVEN plasma observations, *Geophys. Res. Lett.*, *42*, doi:10.1002/2015GL065218.
Mahaffy, P. R., M. Benna, M. Elrod, R. V. Yelle, S. W. Bougher, S. W. Stone, and B. M. Jakosky (2015), Structure and composition of the neutral upper atmosphere of Mars from the MAVEN NGIMS investigation, *Geophys. Res. Lett.*, *42*, doi:10.1002/2015GL065329.
McFadden, J. P., R. Livi, J. Luhmann, J. Connerney, D. Mitchell, C. Mazelle, L. Andersson, and B. Jakosky (2015), Structure of the Martian ionosphere and atmospheric loss: MAVEN STATIC first results, Lunar Planet. Sci. Conf., Abstract 2899.
Mitchell, D. L., R. P. Lin, C. Mazelle, H. Rème, P. A. Cloutier, J. E. P. Connerney, M. H. Acuña, and N. F. Ness (2001), Probing Mars' crustal magnetic field and ionosphere with the MGS Electron Reflectometer, *J. Geophys. Res.*, *106*(E), 23,419–23,428, doi:10.1029/2000JE001435.
Nier, A. O., and M. B. McElroy (1977), Composition and structure of Mars' upper atmosphere: Results from the neutral mass spectrometers on Viking 1 and 2, *J. Geophys. Res.*, *82*, 4341–4349, doi:10.1029/JS082i028p04341.
Pätzold, M. S., B. Tellman, B. Häusler, D. Hinson, R. Scaa, and G. L. Tyler (2005), A sporadic third layer in the ionosphere of Mars, *Science*, *310*, 837–839.
Paxton, L. J., and D. E. Anderson (1992), Ultraviolet remote sensing of Venus and Mars, in *Venus and Mars: Atmospheres, Ionospheres, and Solar Wind Interactions*, *Geophys. Monograph*, vol. 66, edited by J. G. Luhmann, M. Tatrallyay, and R. O. Pepin, pp. 113–190, doi:10.1029/GM066p0113.
Rahmati, A., D. E. Larson, T. E. Cravens, R. J. Lillis, P. A. Dunn, J. S. Halekas, J. E. Connerney, F. G. Eparvier, E. M. B. Thiemann, and B. M. Jakosky (2015), MAVEN insights into oxygen pickup ions at Mars, *Geophys. Res. Lett.*, *42*, doi:10.1002/2015GL065262.
Schneider, N. M., et al. (2015a), MAVEN IUVS observations of the aftermath of the Comet Siding Spring meteor shower on Mars, *Geophys. Res. Lett.*, *42*, 4755–4761, doi:10.1002/2015GL063863.
Schneider, N. M., et al. (2015b), Discovery of diffuse aurora on Mars, *Science*, doi:10.1126/science.aad0313, in press.
Yung, Y. L., J. S. Wen, J. P. Pinto, M. Allen, K. K. Pierce, and S. Paulson (1988), HDO in the Martian atmosphere—Implications for the abundance of crustal water, *Icarus*, *76*(1), 146–159, doi:10.1016/0019-1035(88)90147-9.